

Microplastic fouling: a gap in knowledge and a research imperative to improve their study by infrared characterization spectroscopy

Mikaël Kedzierski<sup>\*a</sup>, Maialen Palazot<sup>a</sup>, Lata Soccalingame<sup>a</sup>, Maria Luiza Pedrotti<sup>b</sup>, Stéphane Bruzaud<sup>a</sup>

<sup>a</sup>Université Bretagne Sud, UMR CNRS 6027, IRDL, F-56100 Lorient, France

<sup>b</sup>Sorbonne Universités, UMR CNRS 7093, LOV, F-06230 Villefranche sur mer, France

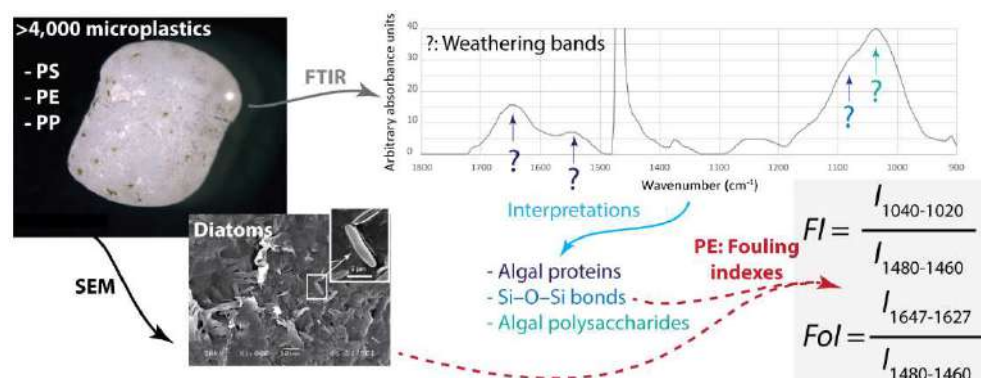
**Corresponding author**

\*E-mail: [mikael.kedzierski@univ-ubs.fr](mailto:mikael.kedzierski@univ-ubs.fr)

## HIGHLIGHTS

- Spectra of weathered microplastics have shown new bands
- This spectral variability was mainly related to only three processes: chemical ageing, organic and inorganic fouling
- Two new polymer indices able to monitor the intensity of (bio)fouling were proposed

## GRAPHICAL ABSTRACT



## ABSTRACT

The marine weathering of microplastics is spectrally characterized by the appearance of new bands that disturb our understanding of the information carried by the spectra. Yet, no

explanation has been provided on the chemical origin of these new bands. Thus, the main objective of this work was to identify the origins of these additional bands. To this end, 4,042 spectra of poly(styrene), poly(ethylene) and poly(propylene) microplastics collected in the Mediterranean Sea, were analysed using principal component analysis. The results showed that the spectral variability was mainly related to only three processes: chemical ageing, organic and inorganic fouling. These processes probably differ from one polymer family to another due to surface affinities. This work has also led to the proposal of two new polymer indices that could be used to monitor the intensity of (bio)fouling. Finally, the development of advanced analyses could also provide information on the nature of the plastisphere.

## **Keywords**

Microplastic, FTIR spectra, Fouling, Plastisphere, Indices

## **1. Introduction**

In the last few years, plastic pollution has become a major environmental and health problem (Avio et al., 2017). This pollution, present from remote and uninhabited polar lands to the heights of Mount Everest, is now considered ubiquitous (Cózar et al., 2017; Lacerda et al., 2019; Napper et al., 2020).

Among the parameters studied to describe microplastic (MP) pollution, the chemical nature of the particles is of paramount importance (Gewert et al., 2017; Imhof et al., 2017; Kedzierski et al., 2022; Wang et al., 2017). Different methods such as pyrolysis-gas chromatography in combination with mass spectrometry (GC/MS) (Doyen et al., 2019; Primpke et al., 2020; Scherer et al., 2020), Raman (Dehaut et al., 2016; Long et al., 2019; Prata et al., 2019) or Infrared (IR) spectroscopy (Huo et al., 2022; Kedzierski et al., 2022; Scherer et al., 2020; Wakkaf et al., 2022), have proven their effectiveness in determining the chemical nature of

MP. Among them, Fourier transform infrared spectroscopy (FTIR) is one of the most widely used.

The appearance of additional bands is part of the classical modifications observed on an FTIR spectrum during the chemical ageing of a polymer (Andrady, 2017, 2011). To assess the level of degradation (mainly due to oxidation by solar UV radiation) by infrared spectroscopy, markers such as carbonyl index (CI) and hydroxyl index (HI) are commonly calculated from these new bands (Julienne et al., 2019). It is commonly accepted that the CI of poly(ethylene) (PE) or poly(propylene) (PP) is correlated in a controlled environment (e.g. climatic chamber) to the level of chemical ageing. This link also exists in air ageing experiments and, to a lesser extent, in aquatic environments (Andrady, 2017, 2011; Zhang et al., 2021).

However, in the marine environment, the appearance of new bands, in particular between 1800 and 1500  $\text{cm}^{-1}$  and between 1200 and 800  $\text{cm}^{-1}$ , disturb the understanding of the information carried by the spectra (Fernández-González et al., 2021; Kedzierski et al., 2019a; Morgado et al., 2021; Syranidou et al., 2017). In addition to disrupting CI and HI calculations, these new bands can lead to errors when spectra of weathered polymers are compared in an automated way with reference databases of virgin polymers (Fernández-González et al., 2021). These new bands are generally ignored and few explanation has yet been provided on their origin (Battulga et al., 2022).

Thus, the main objective of this work was to identify these additional bands and their origins. Then, based on this new knowledge, different potential applications for the survey of the plastisphere was proposed.

## **2. Materials and methods**

### **2.1. Sample collection**

Microplastic samples were collected in the Mediterranean Sea waters during the Tara Expedition which was conducted between June and November 2014 (Kedzierski et al., 2019b). Sampling was conducted using a 4.4 m long manta net (mesh size: 333  $\mu\text{m}$ ; net opening: 16 x 60 cm), in 124 sites which were selected based on ocean colour satellite images supplied by ACRI-ST and analysed with the Mercator circulation model. Metadata such as geographical coordinates or date of sampling are available at Zenodo Data Publisher (DOI/10.5281/zenodo.6551501.svg). At each site, the manta net was towed on the sea surface for ca. 60 min behind the boat at an average speed of 2.5 knots, enabling thus the filtration of around 507  $\text{m}^3$  of seawater surface.

## **2.2. Laboratory preparations**

In the laboratory, the samples were transferred into Petri dishes. Floating plastic debris were carefully removed from other components to separate plastic particles, zooplankton and organic tissues. This process was done using a light box and a dissecting stereomicroscope to observe the sample content under high light contrast and each sample was double-checked to ensure the removal of all the smallest and/or transparent plastic particles. Thus, MP were rinsed with water, but had not undergone a digestion process. The Petri dishes containing the microplastics were dried at 50  $^{\circ}\text{C}$  for 24 h in an oven.

From 75,000 plastic items identified, a total of 15,654 particles, larger than 315  $\mu\text{m}$  from 55 selected sites, were wet sieved by size class ([5-2 mm], [2-1 mm], [1-0.5 mm], [0.5-0.315 mm]). Then, they were transferred to 96-well microplates and named with a unique identifier at the Institut de Recherche Dupuy de Lôme (IRD, Lorient, France) (Kedzierski et al., 2019b). The MP were then stored at room temperature and hygrometry.

## **2.3. Fourier-transform infrared spectroscopy (FTIR)**

The particles spectra were acquired using an Attenuated Total Reflection Fourier Transform Infrared spectrometer (ATR-FTIR Vertex70v, Bruker). All spectra were recorded in absorbance mode in the 4,000-600  $\text{cm}^{-1}$  region with a resolution of 4  $\text{cm}^{-1}$  and 16 scans. Each piece of plastic was placed onto the germanium cristal (ATR Golden Gate; beam penetration at 1000  $\text{cm}^{-1}$ : 0.66  $\mu\text{m}$ ), and one side per microplastic was acquired. After each analysis, the sample holder was cleaned with ethanol. The sample chamber was also cleaned out with a vacuum cleaner after every sixty analyses.

#### **2.4. Determination of the chemical nature**

FTIR spectra had already been analysed in previous studies, using the POSEIDON (Plastic pOllutionS ExtractiOn, DetectiOn and aNalysis) software which is free and open source software (Kedzierski et al., 2022, 2019a, 2019b). This software was developed in the R 3.1.2 environment (The R Core Team, 2019).

Two pre-processing steps were performed: baseline correction, followed by spectrum normalisation (Kedzierski et al., 2019a; Liland, 2015). The machine learning process was carried out using  $k$ -nearest neighbour classification (Ripley, 1996; Venables et al., 2002). The learning database consisted of 969 spectra of MP and other particles (natural organic materials) collected during the 2014 Tara scientific campaign. During the identification step, if all  $k$ -nearest neighbours belonged to the same category, the spectrum was directly identified; otherwise the category of the spectrum was determined according to the nearest category among the  $k$ -nearest neighbours. If it was not possible to obtain more than two neighbours belonging to the same category, then the spectrum was automatically classified as "unknown". In order to test the accuracy of the final classification, a two-step checking was carried out involving a hierarchical cluster analysis and a principal component analysis. Then, the average spectrum of each generated subcluster was calculated and checked. If the average

spectrum of a subcluster did not match the cluster, the spectrum or group of spectra was manually identified and, possibly, reassigned to another class.

Thus, the chemical nature of 4,723 spectra was analysed by POSEIDON and among them, 131 spectra of poly(styrene) (PS), 2851 of poly(ethylene) (PE) and 1042 of poly(propylene) (PP) were identified (Kedzierski et al., 2022, 2019a).

## **2.5. Statistical analysis**

The principal component analysis (PCA, variance-covariance matrix) was performed using PAST software (Hammer et al., 2001). The scores obtained for each of the spectra were then corrected so that the origin of the factorial map (0,0) corresponded to the spectrum of the virgin reference polymer.

Parametric correlation coefficient between main bands was also calculated with PAST software using Pearsons's test (Hammer et al., 2001).

## **2.6. Scanning Electron Microscope**

Plastic surface imaging was performed by using a Scanning Electron Microscope (SEM; JEOL 6460-LV) at 20 kV in secondary electrons image (SEI). The chemical analysis was carried out using backscattered electron images (BSE) coupled with Energy Dispersive X-ray spectroscopy (EDS; Oxford Instrument X-ACT SATW 10mm2) at 20 kV.

## **2.7. Reference spectra**

FTIR spectra data bank of different laboratory objects has been established. Among the spectra, those of PS, PE and PP were selected to be used as reference (non-aged polymer) (Primpke et al., 2018). These reference spectra were typical of what was described in the literature for these kinds of polymers (Lobo and Bonilla, 2003; Schröder et al., 1989). In order to safely identify spectral markers linked to potential bio and organic fouling, different spectra

were acquired and compared with literature. First, the spectrum of an alga (*Ascophyllum sp.*) collected at Kernevel harbor (GPS coordinates: 47.7173, -3.3666; France) located in the Bay of Lorient was obtained and used as a proxy. It is important to note that although derived from a macroalgal sample, the spectrum showed the main bands described for microalgae (Dean et al., 2010; Murdock and Wetzel, 2009; Quilès et al., 2010; Schmitt et al., 1995). It is for example the case of diatoms which are quite classical microalgae in the biofouling process of microplastics (Amaral-Zettler et al., 2020). It is therefore possible to use this algal spectrum as a proxy for biofouling.

Sedimentation in the Mediterranean Sea is essentially detrital with inputs of clay minerals, calcite, quartz and feldspar (Tribble and Wilkens, 1999). Among these particles suspended in the aquatic environment, quartz and clay particles can adhere to the surface of microplastics (Meng et al., 2021, Kowalski et al., 2016). A preliminary comparison between the spectra of quartz and clay particles revealed bands similar to some of the additional bands visible in the spectra of microplastics collected during the expedition. Consequently, as the mineralogical composition on the surface of microplastics is probably different from that of seawater, we chose to rely on reference spectra. Thus, spectra of quartz and clay (Talc) were extracted from the RRUFF™ Project database (<https://rruff.info/>) (Lafuente et al., 2015). These two spectra were combined to simulate an inorganic fouling consisting of a mixture of clay and quartz. Thus, the synthetic spectrum obtained presented bands characteristic bands of both clay and quartz.

Three spectra of MP among those collected during the 2014 campaign in the Mediterranean Sea were selected for the particularly high intensity of the additional bands. The purpose of these spectra was to illustrate the appearance of new bands in the most readable way possible. These spectra were: TM0101A11 (poly(styrene)), TM0079B9 (poly(ethylene)), and TM0075E10 (poly(propylene)). Another sample named TM0048A3 (poly(ethylene)) was also

selected to illustrate the specific aspect of the organic fouling. These spectra were named in this publication after the nomenclature developed during this campaign (Kedzierski et al., 2019b).

Through the PCA loadings, the spectrum scores were then calculated and the samples projected into the factorial maps of the Tara samples.

### 3. Results and discussion

#### 3.1. Spectral markers of talc, quartz, and algae FTIR spectra

The spectrum of talc was characterized by bands caused by O-H stretching that occurs at 3677  $\text{cm}^{-1}$  (Fig. 1) (Ramamoorthy et al., 2021; Schroeder, 2002; Yi et al., 2019). The tetrahedral sheet resulted in a sharp band at 1003  $\text{cm}^{-1}$  (Ramamoorthy et al., 2021; Schroeder, 2002). Finally, two assignments prevailed in the literature of the band located at 665  $\text{cm}^{-1}$ : the stretching vibration of Si–O–Mg (Ramamoorthy et al., 2021; Yi et al., 2019) or the libration modes of the Mg–OH in talc end-member (Dokmai et al., 2021; Schroeder, 2002). With regard to the presence of quartz, the Si–O–Si bonds resulted in bands at 1163  $\text{cm}^{-1}$  and 1070  $\text{cm}^{-1}$  (Anbalagan et al., 2010). The latter was partially masked by the band at 1003  $\text{cm}^{-1}$  of talc. The stretching of Si–O bonds was also responsible for the band at 1070  $\text{cm}^{-1}$ , but also for the band at 798  $\text{cm}^{-1}$  (Anbalagan et al., 2010).

Concerning the spectrum of the algae (*Ascophyllum sp.*), the broad band between 3650 and ca. 3000  $\text{cm}^{-1}$  could be attributed to both O–H and N–H stretching vibrations owing to the presence of water and proteins (Murdock and Wetzel, 2009; Schmitt et al., 1995). Bands caused by the stretching of  $-\text{CH}_3$  (2968  $\text{cm}^{-1}$ ),  $-\text{CH}_2$  (2923  $\text{cm}^{-1}$ ),  $-\text{CH}_2$  and  $-\text{CH}_3$  (2861  $\text{cm}^{-1}$ ), and related to the presence of membrane lipids in algae, were also observed (Giordano et al., 2001; Murdock and Wetzel, 2009; Quilès et al., 2010; Schmitt et al., 1995). The ester C=O stretching of membrane phospholipids gave rise to a small band around 1740  $\text{cm}^{-1}$  (Dean

et al., 2010; Murdock and Wetzel, 2009; Quilès et al., 2010). This band could be interesting to study more precisely in the future as it could be associated with the metabolism of microorganisms on the surface of microplastics (Battulga et al., 2022). Algal proteins show up as several bands attributed to the peptide C=O stretching mode (amide I, 1637  $\text{cm}^{-1}$ ), N–H scissoring (amide II, 1541  $\text{cm}^{-1}$ ),  $-\text{CH}_2$  and  $-\text{CH}_3$  stretching (1456  $\text{cm}^{-1}$ ),  $-\text{CH}_2$  and  $-\text{CH}_3$  scissoring and C–O stretching (1396  $\text{cm}^{-1}$ ), and finally to P=O stretching (1225  $\text{cm}^{-1}$ ) (Dean et al., 2010; Giordano et al., 2001; Murdock and Wetzel, 2009). The stretching of C–O–C bonds from polysaccharides resulted in a broad band located between 1200 and 950  $\text{cm}^{-1}$ , whose maximum intensity was observed ca. 1045  $\text{cm}^{-1}$  (Dean et al., 2010; Murdock and Wetzel, 2009). Its large intensity should partially be due to a strong overlap with silicate related bands (Giordano et al., 2001; Stehfest et al., 2005). This is the case, for example, with diatoms whose cell wall is composed of silica and whose spectrum features an intense band located around 1075-1060  $\text{cm}^{-1}$  (Murdock and Wetzel, 2009). This can be confused with a fouling mixing both organic and inorganic fouling.

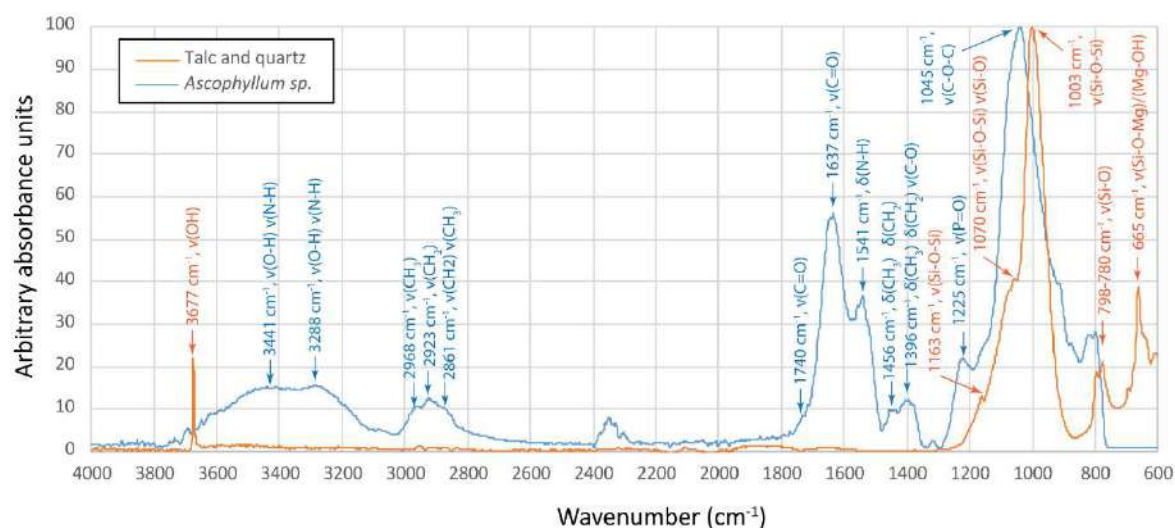


Fig. 1. Spectral markers arising from both organic and inorganic fouling of microplastics.

### 3.2. Identification of spectral markers occurring during ageing in the Mediterranean Sea through three samples

### 3.2.1. Poly(styrene)

The spectrum of the PS reference was characterized by bands associated with a mono-substituted aromatic compound (Fig. 2.a) (Lobo and Bonilla, 2003; Socrates, 2004). Normal aromatic absorption was characterized by strong bands at 3062 and 3027  $\text{cm}^{-1}$ , corresponding to  $=\text{C}-\text{H}$  stretching, and bands at approximately 1604, 1495 and 1454  $\text{cm}^{-1}$  related to aromatic ring stretching vibrations. Very strong bands at 755 and 698  $\text{cm}^{-1}$  corresponded to  $\text{C}-\text{H}$  out-of-plane vibration and a ring out-of-plane deformation, respectively. The  $\text{C}-\text{H}$  stretching vibration of the aliphatic group was highlighted by bands at 2926 and 2850  $\text{cm}^{-1}$ . The other bands, between 1400 to 800  $\text{cm}^{-1}$ , correspond to the typical positions of the bands of aliphatic  $\text{C}-\text{H}$  deformation vibrations.

The formation of hydroxyl bonds was a characteristic of chemical ageing of the polymer. In the case of the spectrum of TM0101A11, the appearance of these bonds resulted in the increase of a very broad band between 3600 and 3000  $\text{cm}^{-1}$ , clearly visible in the spectrum of PS aged at sea (Andrady and Pegram, 1991; Mailhot and Gardette, 1992). Then, a broad band between 1800 and 1700  $\text{cm}^{-1}$  was clearly visible. This broad band had different maxima and shoulders at 1780, 1733, 1720 and 1709  $\text{cm}^{-1}$ . These bands correspond to the carboxyl groups, esters and gamma-lactones of different degradation products (e.g. acetic acid, benzoic acid, carboxylic acid) formed when exposed to UV (Hüffer et al., 2018; Mailhot and Gardette, 1992). Finally, a broad band centered at approximately 1640  $\text{cm}^{-1}$  ( $\text{C}=\text{C}$  or  $\text{C}=\text{O}$  groups) could be highlighted in the microplastic spectra (Fernández-González et al., 2021).

### 3.2.2. Poly(ethylene)

Chemically, poly(ethylene) can be assimilated to a long chain of methylene groups with two terminal methyl groups (Lobo and Bonilla, 2003; Socrates, 2004). Consequently, the FTIR spectrum of the PE reference was very simple (Fig. 2.b). Two very strong bands caused by

stretching vibrations show up on the spectrum at 2916 ( $\nu_{asym}$   $-CH_2$ ) and 2848  $cm^{-1}$  ( $\nu_{sym}$   $-CH_2$ ). Bending modes of  $-CH_2$  groups appeared as two doublets. The first one, assigned to  $-CH_2$  scissoring, was located at 1471 and 1463  $cm^{-1}$ , and the second one, to  $-CH_2$  rocking, at 730 and 720  $cm^{-1}$ . In the particular case of a PE exhibiting a significant branching level, two additional weak bands, typical of low-density poly(ethylene) (LDPE), could be observed at 1376 and 1363  $cm^{-1}$ .

The changes observed in PE microplastic (TM0079B9) were relatively typical (Fernández-González et al., 2021). First, a broad band corresponding to the hydroxyl groups appeared between 3600 and 3200  $cm^{-1}$ . However, this band was rather weak. Between 1800 and 1600  $cm^{-1}$ , different bands related to chemical ageing were assessed and could be related to peresters or free carboxylic acids (1772  $cm^{-1}$ ), peracids (1749  $cm^{-1}$ ), aldehydes (1734  $cm^{-1}$ ), carboxylic acids (1716  $cm^{-1}$ ),  $\gamma$ -ketoacids and acid group (1749  $cm^{-1}$ ), and ketones (1683  $cm^{-1}$ ) (Fernández-González et al., 2021; Yagoubi et al., 2015).

### 3.2.3. Poly(propylene)

The FTIR spectra of the PP reference featured strong bands at 2952 and 2920  $cm^{-1}$  due to  $-CH_3$  stretching (symmetric and asymmetric) on the one hand, and to  $-CH_2$  stretching (*sym* and *asym*) on the other hand (Fig. 2.c) (Chércoles Asensio et al., 2009; Socrates, 2004). Bands of medium intensity were then observed at 2870 and 2841  $cm^{-1}$ . These bands were equally associated with  $-CH_3$  and  $-CH_2$  symmetric and asymmetric stretching. Medium intensity bands at 1458 and 1378  $cm^{-1}$  were respectively associated with  $-CH_2$  and  $-CH_3$  scissoring.  $-CH_3$  rocking and C-C backbone stretching were located at 1169 and 975  $cm^{-1}$ .  $-CH_3$  rocking and  $-CH_2$  wagging could be seen at 1001  $cm^{-1}$ . Finally, three other bands could be identified at 901 and 840  $cm^{-1}$  ( $-CH_2$  rocking) and 809  $cm^{-1}$  (stretching of the C-C backbone).

249 The ageing of PP leads to the appearance of ageing bands similar to those observed for PE  
250 (Fernández-González et al., 2021). Thus, the hydroxyl bands were found between 3600 and  
251 3200  $\text{cm}^{-1}$ . They were clearly visible in the spectrum of the microplastic (TM0075E10), but  
252 partially hidden by the background. Finally, a serie of carbonyl bands can be observed  
253 between 1800 and 1680  $\text{cm}^{-1}$ . Their assignments were given in the PE previous section.

254

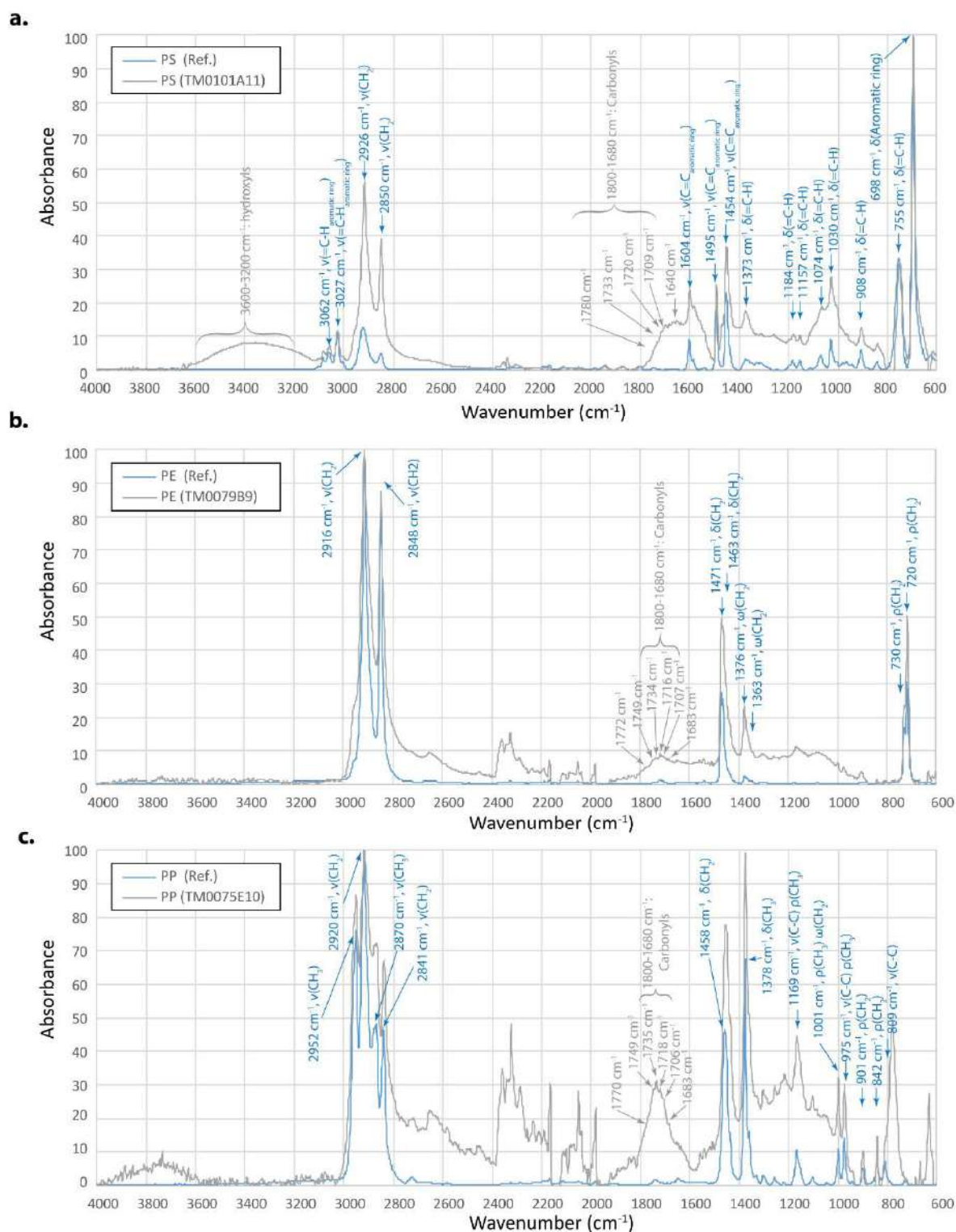
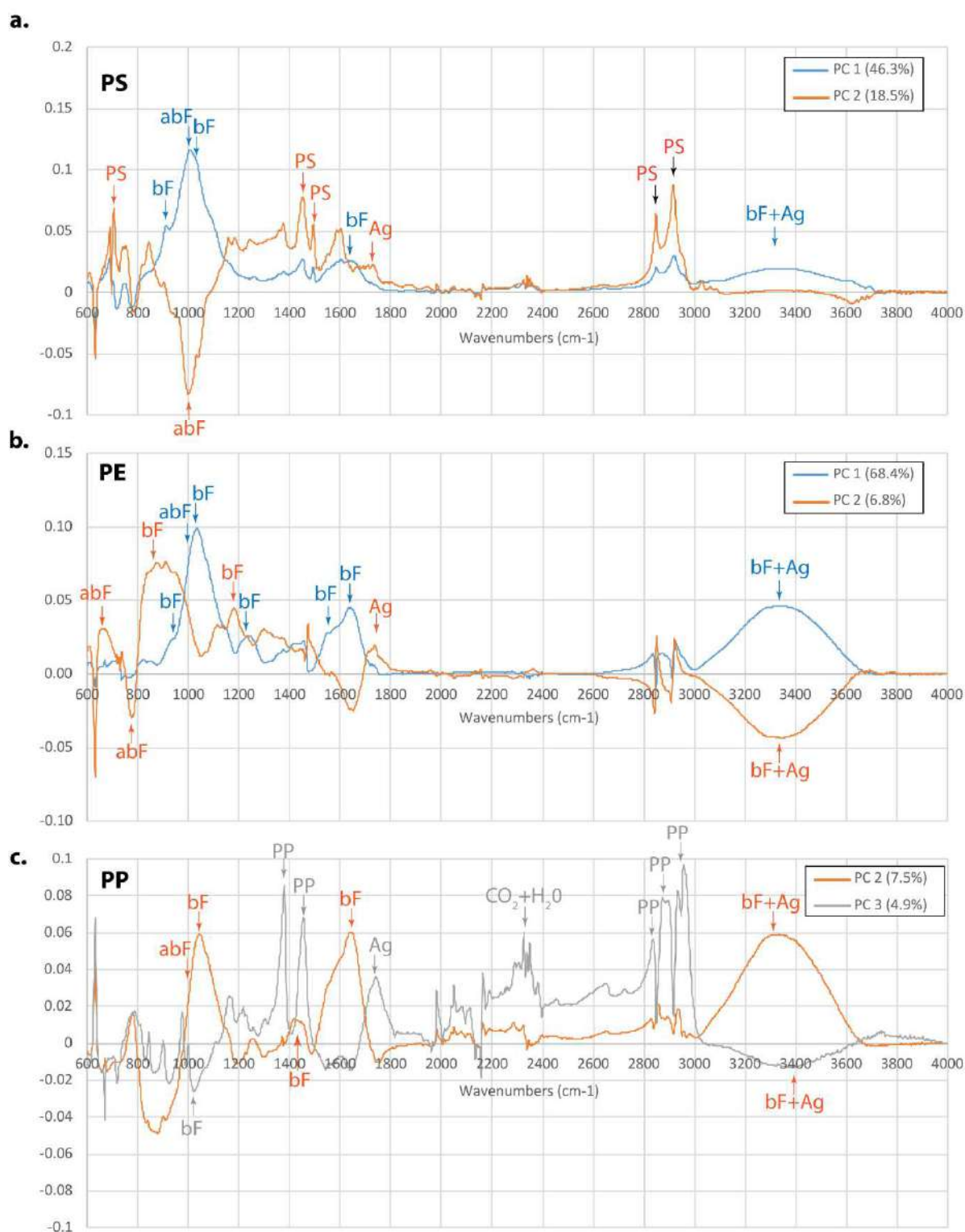


Fig. 2. Spectra of reference polymers (pristine and selected from the Tara mission data set). a. PS: poly(styrene). b. PE: Poly(ethylene). c. PP: poly(propylene).

### 3.3. Spectral variability of PS, PE and PP microplastics collected in the Mediterranean Sea

The first three PCA loadings of the PS, PE and PP spectra are presented in Fig. 3. Their analysis allowed to identify, for each principal component (PC), the wavenumbers with the most variance.

For PS, the first component PC1 accounted for 46.3% of the total variance (Fig. 3.a). Through loadings analysis, this PC1 describes first the growth of bands corresponding to biotic and abiotic fouling. Thus, it was necessary to note the significant weight given to the wave numbers corresponding to the bands centered at 1045 and at 1003  $\text{cm}^{-1}$ . The second component (18.5%) was characterized by the significant weight of the band at 1003  $\text{cm}^{-1}$  (inorganic fouling) and to a lesser extent of the bands between 1750-1700  $\text{cm}^{-1}$  (chemical ageing). Finally, PC3 (10.9%) was less relevant than the two previous ones. The loadings of PC1 and PC2 were therefore further analyzed for the PCA of PS. A high value on the PC1 axis indicated significant organic or inorganic fouling. A high value on the PC2 axis indicated significant chemical ageing, while a low value on this axis indicated significant inorganic fouling. The projection of the reference samples on the factorial map confirmed this analysis.



274

275 Fig. 3. Principal Component Analysis (PCA) loadings of the poly(styrene) (PS),  
 276 poly(ethylene) (PE) and poly(propylene) (PP). The components chosen for these PCA allow  
 277 to highlight the different types of weathering occurring in the natural environment. a. PC1

278 (68.4%) and PC2 (6.8%) were selected for PS. b. PC1 (68.4%) and PC2 (6.8%) were selected  
279 for PS. c. PC2 (7.5%) and PC3 (4.9%) were selected for PP. See explanation in the text.

280 For PE, PC1 accounted for 68.4% of the total variance and, as for PS, highlighted the bands  
281 related to fouling (Fig. 3.b). Thus, a high value on the x-axis (PC1) indicated intense fouling.  
282 PC2 (6.8%) was less informative because of the highlighting of the bands between 1000 and  
283 800  $\text{cm}^{-1}$ . PC3 was preferred because it allowed to highlight both information in terms of  
284 fouling, and chemical ageing. Thus, the higher the score, the greater ageing of the polymer,  
285 and in contrast, the lower y-axis value, the greater fouling of the polymer. This distribution  
286 was confirmed by the projection of the reference samples.

287 Finally, for PP, PC1 (70.0%) reflected baseline variations in the FTIR spectra (Fig. 3.c). It  
288 will therefore not be retained for the analysis. The PC2 (7.5%) characterized the state of  
289 fouling. Thus, spectra with large bands related to fouling had a high value on this axis. PC3  
290 (4.9%) highlighted samples with significant chemical ageing, fouling, but also bands related  
291 to atmospheric  $\text{CO}_2$  and  $\text{H}_2\text{O}$ . Thus, a high value on the x-axis (PC2) indicated significant  
292 fouling. A high value on the y-axis (PC3) indicated a high degree of chemical ageing. On the  
293 contrary, a value close to 0 reflects organic fouling. The projection of the reference samples  
294 also confirmed this interpretation.

295 The PS spectra were spread on the factorial map following a trifid pattern (Fig. 4.a). Most of  
296 the spectra were clustered in a zone labelled  $\omega$ . The average spectrum of this zone was  
297 characterized by additional bands of moderate intensity between 1700-1500 and 1200-1000  
298  $\text{cm}^{-1}$ . These bands could be attributed to biofouling. Beyond the  $\omega$  zone, three patterns could  
299 be identified. These patterns reflected progressive modifications of the spectra according to  
300 particular bands. The  $\alpha$  pattern was characterized by spectra showing increasingly intense  
301 carbonyl bands (between 1800 and 1700  $\text{cm}^{-1}$ ). However, it should be noticed that these bands  
302 were not very differentiated on the spectra, probably because of the superposition in the same

spectral area of these bands associated with chemical ageing with those associated with biofouling. Nevertheless, this pattern corresponds to the progressive increase in chemical ageing accompanied by a more or less intense organic fouling. The  $\beta$  pattern was characterized by spectra with bands related to a relatively intense organic fouling. Finally, the  $\gamma$  pattern was dominated by spectra showing a strong band at  $1003\text{ cm}^{-1}$ , indicative of inorganic fouling. The density of the plotted spectra on the PCA decreases beyond the  $\alpha$ ,  $\beta$  or  $\gamma$  patterns. Between these areas of higher spectra density there were others for which little or no spectrum was projected. For example, no spectrum was projected onto the origin of the axes (zone I). This implied that all the spectra of the collected MP were therefore different from the reference spectrum and none of them can be considered as unaged PS. Zone II corresponded to an area with no point on the factorial map and indicated that it was unlikely that a PS spectrum could have a strong carbonyl band without also having a more or less significant organic fouling. This could mean that chemical ageing and organic fouling processes occur together in the natural environment, but with varying degrees. Zone III appeared between the  $\alpha$  and  $\beta$  patterns. This also could mean that when the bands associated with biofouling were very intense, it was more difficult to also have very intense carbonyl bands. Zone IV, visible between the  $\beta$  and  $\gamma$  patterns, was also characterized by a near absence of spectra. This could indicate that spectra with intense bands related to both significant bio and inorganic fouling were more unlikely. It is indeed possible that when the fouling of the surface is important, the MP are more protected from UV rays and age less chemically. Finally, zone V corresponded to an area without a point on the factorial map that can probably be explained by the component loadings. Indeed, since both components were sensitive to the band at  $1003\text{ cm}^{-1}$  (PC1 in positive, PC2 in negative), no spectrum presenting the characteristics of an inorganic fouling can be projected into zone V. And as no other band had

significant weight on the negative PC2, no other type of spectrum could be projected below 0 on the y-axis.

The distribution of the spectra on the PCA was different for the PE and PP as they clearly showed a bifid pattern (Fig. 4.b and c). Thus, the  $\alpha$  and  $\beta$  branches were well present, but the  $\gamma$  branch, specific to inorganic fouling was absent while it was present on the PCA of the PS spectra. Thus, for these two polymers, inorganic fouling seemed to be rare or very weak. In the case of PE, the average spectrum of the Zone I spectra showed distinct and well-marked, but weak carbonyl bands. Few spectra were found in this zone (0.7%), indicating that most of the PE spectra showed additional bands compared to the unaged PE reference (Fig. 4.b). For the  $\omega$  region, corresponding to most of the spectra (30.7%), bands associated with moderate biofouling appeared in addition to those of chemical ageing. The average spectrum of the  $\alpha$ -pattern was characterized by strong carbonyl bands and less pronounced biofouling-related bands. In contrast, the average spectrum of the  $\beta$ -pattern was characterized by strong biofouling-related bands and weaker carbonyl bands. In the case of PP, the average spectrum of the  $\omega$  zone indicated low fouling and low chemical ageing (Fig. 4.c). The average spectrum of the  $\alpha$  pattern indicated stronger chemical ageing while that of the  $\beta$  pattern indicated strong organic fouling. For these two polymers the interpretations of zones II and III were similar to those of PS. Zone VI implied that inorganic fouling was low for both chemical families of polymers. Caution should be exercised in interpreting these trends. It is possible that chemical ageing and fouling may occur simultaneously or sequentially. For the moment, we have no diagnostic element to distinguish between these two cases. For the bands between 1800 and 1700  $\text{cm}^{-1}$ , it is also difficult at this stage to discriminate between the chemical ageing part and the organic fouling part. There is currently a lack of understanding of these trends and new experiments need to be conducted.



Fig. 4. Factorial map of poly(styrene) (PS), poly(ethylene) (PE) et poly(propylene) (PP) spectra. a. PS triffid pattern. b. PE biffid pattern. c. PP biffid pattern. See explanation in the text.

### 3.4. Characterisation of the plastisphere with a fouling index

We propose to use these bands to create an index to describe the fouling of (micro)plastics in the marine environment. For this purpose, the broad band between 1200 and 900  $\text{cm}^{-1}$  which peaks show up between 1040 and 1020  $\text{cm}^{-1}$  were first considered. This broad band resulted from the overlay of bands at 1070  $\text{cm}^{-1}$ , 1045  $\text{cm}^{-1}$ , 1003  $\text{cm}^{-1}$ . It should be noted that PE does not exhibit a significant band in this frequency range. Since this polymer is the most common in many environmental media and matrices, it was the best candidate for monitoring fouling extent by infrared spectroscopy (Erni-Cassola et al., 2019; Kedzierski et al., 2022; Schwarz et al., 2019). The most common denominator of the PE indices (*i.e.* carbonyl index, hydroxyl index, vinyl index) is generally the intensity of the band at 1470  $\text{cm}^{-1}$  (Julienne et al., 2019). Therefore, we proposed a fouling index (FI) that could be calculated as follows (Kedzierski et al., 2022):

$$FI = \frac{I_{1040-1020}}{I_{1480-1460}} (1)$$

With  $I_{1040-1020}$  mainly corresponding to the bands of algal polysaccharides, as well as to a lesser extent to Si-O-Si bonds, and  $I_{1480-1460}$  corresponding to  $-\text{CH}_2$  scissoring of PE.

Was it possible to refine the monitoring of fouling by resolving inorganic from organic fouling? The band at 1003  $\text{cm}^{-1}$  reflecting inorganic fouling and the band at 1045  $\text{cm}^{-1}$  reflecting organic fouling were better expressed, and thus appeared to be good candidates. Nevertheless, these two bands showed a significant correlation ( $r=0.96$ ), implying that these two bands were too spectrally close to each other (Fig. 5). The same applied to the band located at 1070  $\text{cm}^{-1}$  which also correlated closely with the other two.

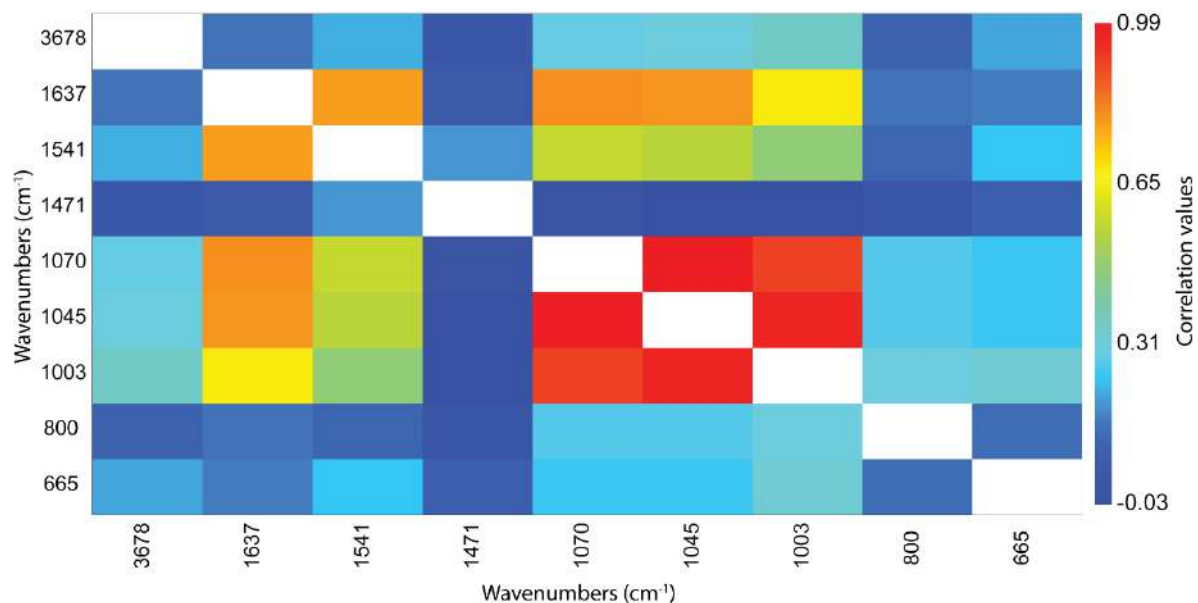


Fig. 5. Parametric correlation coefficient (Pearson's  $r$ ) of different spectral bands. The absorbance values at 1003, 1045 and 1070  $\text{cm}^{-1}$  are highly correlated probably due to the overlap of these bands.

The silicate bands at 3678, 800 and 665  $\text{cm}^{-1}$  were too weakly expressed or readable on the spectra to be useful. Thus, an index of inorganic fouling did not seem to be possible for the moment without using, for example, a Gaussian peak fitting method. For biofouling, on the other hand, the band at 1637  $\text{cm}^{-1}$  ( $\nu(\text{C}=\text{O})$ , protein) was very interesting and allowed us to propose the following organic fouling index:

$$F_oI = \frac{I_{1647-1627}}{I_{1480-1460}} \quad (2)$$

With  $I_{1647-1627}$  corresponding to amide I band of algal proteins.

The ranking of the PE MP spectra according to the importance of  $F_oI$  illustrated the increase of organic fouling (Fig. 6.a): for 59% of the PE spectra the  $F_oI$  index was below 0.2. In this case, the fouling was visually characterized by faint bands indicating a weak organic fouling. Between 0.2 and 0.4 (32% of the PE spectra), bands were clearly visible between 1300 and 900  $\text{cm}^{-1}$  (i.e. bands attributed to the stretching of  $\text{C}=\text{O}$  bonds from algal proteins).

Approximately 9% of the spectra showed a F<sub>o</sub>I greater than 0.4, indicating significant organic fouling. The fact that the majority of MP have a low F<sub>o</sub>I could be an indication that these MP had been present for a relatively "short time" in the natural environment. This would suggest a relatively short drift time of MP on the ocean surface, which could be of the order of a few dozen days according to experimental data (Fazey and Ryan, 2016). This short time scale (a few weeks) also agrees with an average residence time of plastics in the Mediterranean Sea between 7 and 90 days (Baudena et al., 2022; Liubartseva et al., 2018; Pedrotti et al., 2022). Another possibility is that the environmental conditions were globally not favorable to biofouling. The sampling season could for example have an impact, the spring-summer period being favourable to organic fouling, the autumn-winter less so. Thus, the application of the FI index on PE samples showed that this index was significantly higher in June than in September-October, thus showing a probable sensitivity to seasonality (Kedzierski et al., 2022). However, in our case, samples were mostly sampled in summer, so from this particular point environmental conditions seem quite favorable to fouling. Another very interesting hypothesis can also be formulated: it is possible that the more intensively a microplastic is biofouled (i.e. with a high F<sub>o</sub>I index), the greater the probability that it will sediment (Fazey and Ryan, 2016; Kooi et al., 2017, 2016; Lobelle and Cunliffe, 2011). Thus, it is possible that the two proposed indices directly reflect the fouling state of the plastic and indirectly its ability to remain on the water surface. However, further investigations are needed to verify this proposition.

Is it possible to determine the nature of the plastisphere present on the polymer surface by the way of the FTIR spectrum? For example, in the case of the TM0048A3 sample, a PE pellet with a moderate F<sub>o</sub>I (0.23), it was possible to observe on its surface areas of green colour (Fig. 6.b). SEM observation revealed the presence of diatoms (*Bacillariophyta*) that had largely colonised the infractuositities (Fig. 6.c). Analysis of the FTIR spectrum showed that in addition

to the band at  $1045\text{ cm}^{-1}$ , a characteristic shoulder is visible at  $1100\text{-}1060\text{ cm}^{-1}$ , reflecting the presence of diatom frustule silica (fig. 6.d) (Murdock and Wetzel, 2009). This diatom fingerprint was visible on a very large number of PE spectra. Thus, from the point of view of FTIR spectra, diatoms could be a good marker of the plastisphere. The study of microalgae by FTIR is well established in the literature (Murdock and Wetzel, 2009). Thus, this scientific literature has shown that it is possible to use FTIR spectra determine the nature of the microalgae (Marcilla et al., 2009; Murdock and Wetzel, 2009), their biomass (Stehfest et al., 2005; Sudhakar and Premalatha, 2015) or the biological responses of the microalgae to their environment (Giordano et al., 2001; Murdock and Wetzel, 2009). In the case of microplastic pollution, diatoms are sensitive to certain additives (Wang et al., 2020). In the slightly different case of an aquatic matrix contaminated with a micropollutant, the toxicity to diatoms may be minimised by the presence of the microplastic (Guo et al., 2020; Hao et al., 2022). The fact that the impact may be expressed in terms of variations in lipid accumulation (Guo et al., 2020), suggests that these variations may also be observed in the FTIR spectra, particularly between  $2968$  and  $2861\text{ cm}^{-1}$ . The question is therefore whether this kind of information could also be exploited from microplastic FTIR spectra. These organisms are also likely to accelerate the transfer of microplastics from the ocean surface to the seabed through their ability to form aggregates (Long et al., 2015). It would therefore be interesting to verify whether there is a link between the proposed indices and their buoyancy. Finally, FTIR spectra of microplastics do not only contain information on microalgae and recently it has been shown that information on fungal species can be extracted from the study of these spectra (Battulga et al., 2022). This again suggests that the amount of information that can be derived from FTIR spectra of microplastics is probably currently under-exploited.

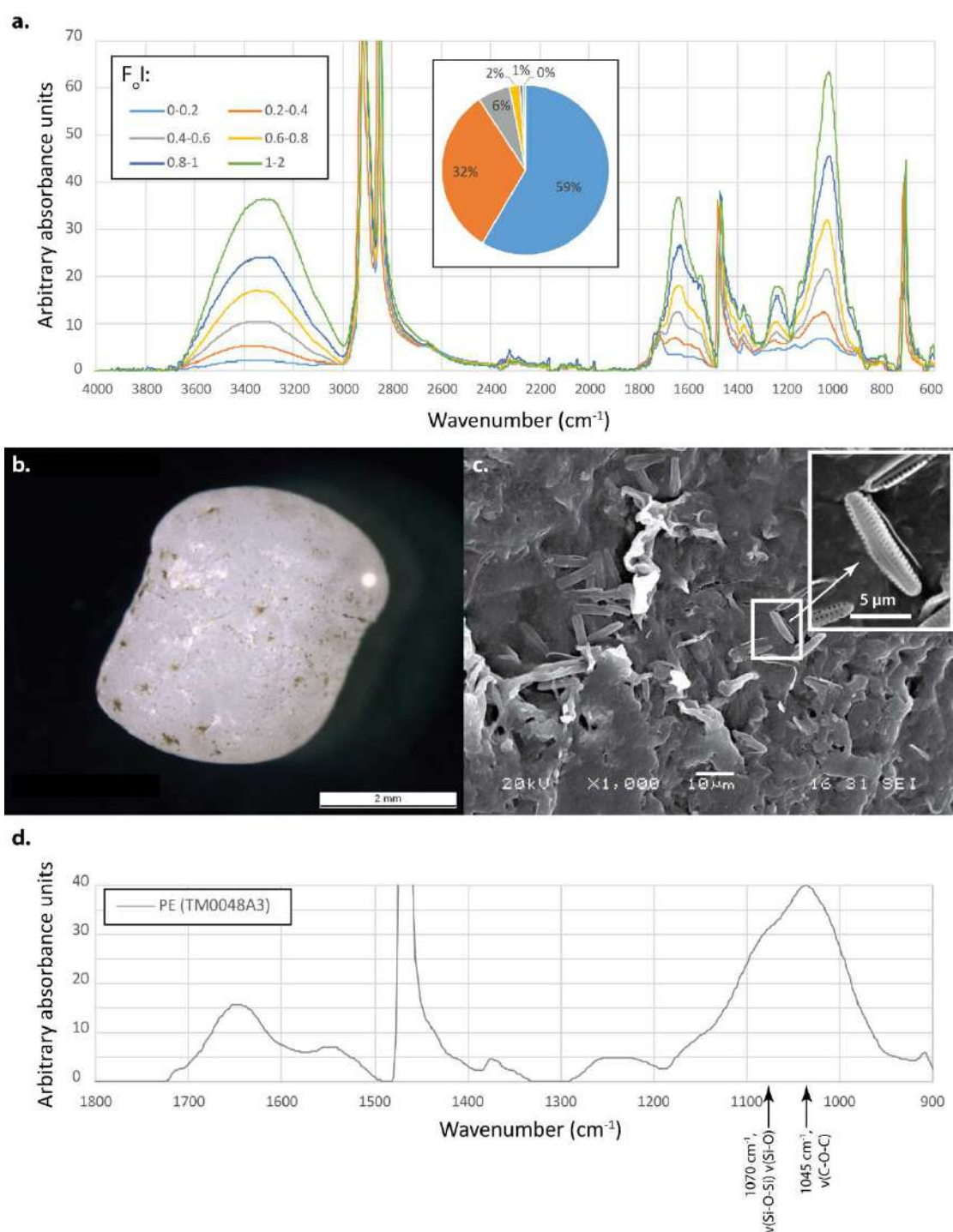


Fig. 6. ATR-FTIR study of the plastisphere. a. Average PE spectra for different FoI index (biofouling index) ranges and percent of PE spectra in these different classes. b. Photograph of TM0048A3. c. SEM photograph of the surface of the sample TM0048A3. Diatoms were clearly visible. d. Infrared spectrum of TM0048A3. The two bands of the spectrum could be the chemical translation of the presence of diatoms.

#### 4. Conclusions

This study showed that the spectral variability of PE, PP and PS MP collected in the Mediterranean Sea was mainly related to three processes: chemical ageing, organic fouling and inorganic fouling. In most cases, these processes lead to relatively limited changes in the spectra, and only a small proportion of the spectra showed advanced changes. Among the identified processes, inorganic fouling was only clearly evident for PS spectra and not for those of PE and PP. This observation tends to show that these processes probably differ from one polymer family to another due to surface affinities. Furthermore, the different patterns observed within the spectra of the same chemical family of plastics could be an indication that the different processes at work could be more or less uncorrelated. The precise mechanisms behind these intra- and inter-chemical group variations remain to be explained and are of utmost interest to better understand the fate of MPs in oceans.

This work has led to the proposal of two new indices: the fouling index (FI) and the organic fouling index (FoI). These two indices provide important and hitherto unexploited information, and raise the question of their use to monitor the intensity of (bio)fouling on the surface of (micro)plastics. The advanced analysis of spectra must also provide information on the nature of the plastisphere (*eg.* diatoms on PE).

Our study focused on most abundant types of polymers, from samples taken from the surface of the Mediterranean Sea. It is therefore relevant to ask the question of the possibility of generalizing these results (*i.e.* to other polymers, other oceans, other environmental matrices). The re-exploitation of existing FTIR spectra databases of MP would enable to rapidly provide answers to these questions.

#### ACKNOWLEDGMENTS

We thank the commitment of the following institutions, persons and sponsors: CNRS, UPMC, LOV, Genoscope/CEA, the Tara Expeditions Foundation and its founders: agnès b.<sup>®</sup>, Etienne Bourgois, Romain Troublé, the Veolia Environment Foundation, Lorient Agglomeration, Serge Ferrari, the Foundation Prince Albert II de Monaco, IDEC, the “Tara” schooner and teams. We thank MERCATOR-CORIOLIS and ACRI-ST for providing daily satellite data during the expedition. We are also grateful to the French Ministry of Foreign Affairs for supporting the expedition and to the countries that graciously granted sampling permission. We would like to thank Marie Emmanuelle Kerros and Maryvonne Henry for their help in the analysis of plastics. Finally, we thank Olivier Sire for his proofreading and useful comments.

## REFERENCES

- Amaral-Zettler, L.A., Zettler, E.R., Mincer, T.J., 2020. Ecology of the plastisphere. *Nat. Rev. Microbiol.* 18, 139–151. <https://doi.org/10.1038/s41579-019-0308-0>
- Anbalagan, G., Prabakaran, A., Gunasekaran, S., 2010. Spectroscopic characterization of indian standard sand. *J. Appl. Spectrosc.* 77, 86–94. <https://doi.org/10.1007/s10812-010-9297-5>
- Andrady, A.L., 2017. The plastic in microplastics: A review. *Mar. Pollut. Bull.* 119, 12–22. <https://doi.org/https://doi.org/10.1016/j.marpolbul.2017.01.082>
- Andrady, A.L., 2011. Microplastics in the marine environment. *Mar. Pollut. Bull.* 62, 1596–1605. <https://doi.org/10.1016/j.marpolbul.2011.05.030>
- Andrady, A.L., Pegram, J.E., 1991. Weathering of polystyrene foam on exposure in air and in seawater. *J. Appl. Polym. Sci.* 42, 1589–1596. <https://doi.org/doi:10.1002/app.1991.070420612>
- Avio, C.G., Gorbi, S., Regoli, F., 2017. Plastics and microplastics in the oceans: From emerging pollutants to emerged threat. *Mar. Environ. Res.* 128, 2–11.

493 <https://doi.org/https://doi.org/10.1016/j.marenvres.2016.05.012>

494 Battulga, B., Kawahigashi, M., Oyuntsetseg, B., 2022. Characterization of biofilms formed on  
 495 polystyrene microplastics (PS-MPs) on the shore of the Tuul River, Mongolia. *Environ.*  
 496 *Res.* 212, 113329. <https://doi.org/https://doi.org/10.1016/j.envres.2022.113329>

497 Baudena, A., Ser-Giacomi, E., Jalón-Rojas, I., Galgani, F., Pedrotti, M.L., 2022. The  
 498 streaming of plastic in the Mediterranean Sea. *Nat. Commun.* 13, 2981.  
 499 <https://doi.org/10.1038/s41467-022-30572-5>

500 Chércoles Asensio, R., San Andrés Moya, M., de la Roja, J.M., Gómez, M., 2009. Analytical  
 501 characterization of polymers used in conservation and restoration by ATR-FTIR  
 502 spectroscopy. *Anal. Bioanal. Chem.* 395, 2081–2096. [https://doi.org/10.1007/s00216-](https://doi.org/10.1007/s00216-009-3201-2)  
 503 [009-3201-2](https://doi.org/10.1007/s00216-009-3201-2)

504 Cózar, A., Martí, E., Duarte, C.M., García-de-Lomas, J., van Sebille, E., Ballatore, T.J.,  
 505 Eguíluz, V.M., González-Gordillo, J.I., Pedrotti, M.L., Echevarría, F., Troublè, R.,  
 506 Irigoien, X., 2017. The Arctic Ocean as a dead end for floating plastics in the North  
 507 Atlantic branch of the Thermohaline Circulation. *Sci. Adv.* 3.  
 508 <https://doi.org/10.1126/sciadv.1600582>

509 Dean, A.P., Sigeo, D.C., Estrada, B., Pittman, J.K., 2010. Using FTIR spectroscopy for rapid  
 510 determination of lipid accumulation in response to nitrogen limitation in freshwater  
 511 microalgae. *Bioresour. Technol.* 101, 4499–4507.  
 512 <https://doi.org/https://doi.org/10.1016/j.biortech.2010.01.065>

513 Dehaut, A., Cassone, A.-L., Frère, L., Hermabessiere, L., Himber, C., Rinnert, E., Rivière, G.,  
 514 Lambert, C., Soudant, P., Huvet, A., Duflos, G., Paul-Pont, I., 2016. Microplastics in  
 515 seafood: Benchmark protocol for their extraction and characterization. *Environ. Pollut.*  
 516 215, 223–233. <https://doi.org/http://dx.doi.org/10.1016/j.envpol.2016.05.018>

517 Dokmai, V., Sinthiptharakoon, K., Phuthong, W., Pavarajarn, V., 2021. Anisotropic  
 518 robustness of talc particles after surface modifications probed by atomic force  
 519 microscopy force spectroscopy. Particuology.  
 520 <https://doi.org/https://doi.org/10.1016/j.partic.2021.04.008>

521 Doyen, P., Hermabessiere, L., Dehaut, A., Himber, C., Decodts, M., Degraeve, T., Delord, L.,  
 522 Gaboriaud, M., Moné, P., Sacco, J., Tavernier, E., Grard, T., Duflos, G., 2019.  
 523 Occurrence and identification of microplastics in beach sediments from the Hauts-de-  
 524 France region. Environ. Sci. Pollut. Res. 26, 28010–28021.  
 525 <https://doi.org/10.1007/s11356-019-06027-8>

526 Erni-Cassola, G., Zadjelovic, V., Gibson, M.I., Christie-Oleza, J.A., 2019. Distribution of  
 527 plastic polymer types in the marine environment; A meta-analysis. J. Hazard. Mater. 369,  
 528 691–698. <https://doi.org/https://doi.org/10.1016/j.jhazmat.2019.02.067>

529 Fazey, F.M.C., Ryan, P.G., 2016. Biofouling on buoyant marine plastics: An experimental  
 530 study into the effect of size on surface longevity. Environ. Pollut. 210, 354–360.  
 531 <https://doi.org/http://dx.doi.org/10.1016/j.envpol.2016.01.026>

532 Fernández-González, V., Andrade-Garda, J.M., López-Mahía, P., Muniategui-Lorenzo, S.,  
 533 2021. Impact of weathering on the chemical identification of microplastics from usual  
 534 packaging polymers in the marine environment. Anal. Chim. Acta 1142, 179–188.  
 535 <https://doi.org/https://doi.org/10.1016/j.aca.2020.11.002>

536 Gewert, B., Ogonowski, M., Barth, A., MacLeod, M., 2017. Abundance and composition of  
 537 near surface microplastics and plastic debris in the Stockholm Archipelago, Baltic Sea.  
 538 Mar. Pollut. Bull. In Press.  
 539 <https://doi.org/https://doi.org/10.1016/j.marpolbul.2017.04.062>

540 Giordano, M., Kansiz, M., Heraud, P., Beardall, J., Wood, B., McNaughton, D., 2001.

541       FOURIER TRANSFORM INFRARED SPECTROSCOPY AS A NOVEL TOOL TO  
 542       INVESTIGATE CHANGES IN INTRACELLULAR MACROMOLECULAR POOLS  
 543       IN THE MARINE MICROALGA CHAETOCEROS MUELLERII  
 544       (BACILLARIOPHYCEAE). J. Phycol. 37, 271–279.  
 545       <https://doi.org/https://doi.org/10.1046/j.1529-8817.2001.037002271.x>

546       Guo, Y., Ma, W., Li, J., Liu, W., Qi, P., Ye, Y., Guo, B., Zhang, J., Qu, C., 2020. Effects of  
 547       microplastics on growth, phenanthrene stress, and lipid accumulation in a diatom,  
 548       Phaeodactylum tricornutum. Environ. Pollut. 257, 113628.  
 549       <https://doi.org/https://doi.org/10.1016/j.envpol.2019.113628>

550       Hammer, Ø., Harper, D.A.T., Ryan, P.D., 2001. Past: Paleontological Statistics Software  
 551       Package for Education and Data Analysis . Palaeontol. Electron. 4, 9.

552       Hao, B., Wu, H., Zhang, S., He, B., 2022. Individual and combined toxicity of microplastics  
 553       and diuron differs between freshwater and marine diatoms. Sci. Total Environ. 853,  
 554       158334. <https://doi.org/https://doi.org/10.1016/j.scitotenv.2022.158334>

555       Hüffer, T., Weniger, A.-K., Hofmann, T., 2018. Sorption of organic compounds by aged  
 556       polystyrene microplastic particles. Environ. Pollut. 236, 218–225.  
 557       <https://doi.org/https://doi.org/10.1016/j.envpol.2018.01.022>

558       Huo, Y., Dijkstra, F.A., Possell, M., Singh, B.B.T.-A. in A., 2022. Plastics in soil  
 559       environments: All things considered. Academic Press.  
 560       <https://doi.org/https://doi.org/10.1016/bs.agron.2022.05.002>

561       Imhof, H.K., Sigl, R., Brauer, E., Feyl, S., Gieseemann, P., Klink, S., Leupolz, K., Loder,  
 562       M.G., Loschel, L.A., Missun, J., Muszynski, S., Ramsperger, A.F., Schrank, I., Speck,  
 563       S., Steibl, S., Trotter, B., Winter, I., Laforsch, C., 2017. Spatial and temporal variation of  
 564       macro-, meso- and microplastic abundance on a remote coral island of the Maldives,

565 Indian Ocean. Mar. Pollut. Bull. 116, 340–347.  
 566 <https://doi.org/10.1016/j.marpolbul.2017.01.010>

567 Julienne, F., Delorme, N., Lagarde, F., 2019. From macroplastics to microplastics: Role of  
 568 water in the fragmentation of polyethylene. Chemosphere 236, 124409.  
 569 <https://doi.org/https://doi.org/10.1016/j.chemosphere.2019.124409>

570 Kedzierski, M., Falcou-Préfol, M., Kerros, M.E., Henry, M., Pedrotti, M.L., Bruzaud, S.,  
 571 2019a. A machine learning algorithm for high throughput identification of FTIR spectra:  
 572 Application on microplastics collected in the Mediterranean Sea. Chemosphere 234,  
 573 242–251. <https://doi.org/10.1016/j.chemosphere.2019.05.113>

574 Kedzierski, M., Palazot, M., Soccalingame, L., Falcou-Préfol, M., Gorsky, G., Galgani, F.,  
 575 Bruzaud, S., Pedrotti, M.L., 2022. Chemical composition of microplastics floating on the  
 576 surface of the Mediterranean Sea. Mar. Pollut. Bull. 174, 113284.  
 577 <https://doi.org/https://doi.org/10.1016/j.marpolbul.2021.113284>

578 Kedzierski, M., Villain, J., Falcou-Préfol, M., Kerros, M.E., Henry, M., Pedrotti, M.L.,  
 579 Bruzaud, S., 2019b. Microplastics in Mediterranean Sea: A protocol to robustly assess  
 580 contamination characteristics. PLoS One 14, e0212088.  
 581 <https://doi.org/10.1371/journal.pone.0212088>

582 Kooi, M., Nes, E.H. van, Scheffer, M., Koelmans, A.A., 2017. Ups and Downs in the Ocean:  
 583 Effects of Biofouling on Vertical Transport of Microplastics. Environ. Sci. Technol. 51,  
 584 7963–7971. <https://doi.org/10.1021/acs.est.6b04702>

585 Kooi, M., Reisser, J., Slat, B., Ferrari, F.F., Schmid, M.S., Cunsolo, S., Brambini, R., Noble,  
 586 K., Sirks, L.-A., Linders, T.E.W., Schoeneich-Argent, R.I., Koelmans, A.A., 2016. The  
 587 effect of particle properties on the depth profile of buoyant plastics in the ocean. Sci.  
 588 Rep. 6, 33882. <https://doi.org/10.1038/srep33882>

589 Lacerda, A.L. d. F., Rodrigues, L. dos S., van Sebille, E., Rodrigues, F.L., Ribeiro, L., Secchi,  
590 E.R., Kessler, F., Proietti, M.C., 2019. Plastics in sea surface waters around the Antarctic  
591 Peninsula. *Sci. Rep.* 9, 3977. <https://doi.org/10.1038/s41598-019-40311-4>

592 Lafuente, B., Downs, R.T., Yang, H., Stone, N., 2015. 1. The power of databases: The  
593 RRUFF project, in: Armbruster, T., Danisi, R.M. (Eds.), . De Gruyter (O), pp. 1–30.  
594 <https://doi.org/doi:10.1515/9783110417104-003>

595 Liland, K.H., 2015. 4S Peak Filling – baseline estimation by iterative mean suppression.  
596 *MethodsX* 2, 135–140. <https://doi.org/10.1016/j.mex.2015.02.009>

597 Liubartseva, S., Coppini, G., Lecci, R., Clementi, E., 2018. Tracking plastics in the  
598 Mediterranean: 2D Lagrangian model. *Mar. Pollut. Bull.* 129, 151–162.  
599 <https://doi.org/https://doi.org/10.1016/j.marpolbul.2018.02.019>

600 Lobelle, D., Cunliffe, M., 2011. Early microbial biofilm formation on marine plastic debris.  
601 *Mar. Pollut. Bull.* 62, 197–200.  
602 <https://doi.org/https://doi.org/10.1016/j.marpolbul.2010.10.013>

603 Lobo, H., Bonilla, J. V., 2003. Handbook of plastics analysis. Taylor & Francis Group, New  
604 York - Basel.

605 Long, M., Moriceau, B., Gallinari, M., Lambert, C., Huvet, A., Raffray, J., Soudant, P., 2015.  
606 Interactions between microplastics and phytoplankton aggregates: Impact on their  
607 respective fates. *Mar. Chem.* 175, 39–46. <https://doi.org/10.1016/j.marchem.2015.04.003>

608 Long, Z., Pan, Z., Wang, W., Ren, J., Yu, X., Lin, L., Lin, H., Chen, H., Jin, X., 2019.  
609 Microplastic abundance, characteristics, and removal in wastewater treatment plants in a  
610 coastal city of China. *Water Res.* 155, 255–265.  
611 <https://doi.org/https://doi.org/10.1016/j.watres.2019.02.028>

612 Maillhot, B., Gardette, J.-L., 1992. Polystyrene photooxidation. 1. Identification of the IR-  
 613 absorbing photoproducts formed at short and long wavelengths. *Macromolecules* 25,  
 614 4119–4126.

615 Marcilla, A., Gómez-Siurana, A., Gomis, C., Chápuli, E., Catalá, M.C., Valdés, F.J., 2009.  
 616 Characterization of microalgal species through TGA/FTIR analysis: Application to  
 617 *nannochloropsis* sp. *Thermochim. Acta* 484, 41–47.  
 618 <https://doi.org/https://doi.org/10.1016/j.tca.2008.12.005>

619 Morgado, V., Gomes, L., Bettencourt da Silva, R., Palma, C., 2021. Validated spreadsheet for  
 620 the identification of PE, PET, PP and PS microplastics by micro-ATR-FTIR spectra with  
 621 known uncertainty. *Talanta* 122624.  
 622 <https://doi.org/https://doi.org/10.1016/j.talanta.2021.122624>

623 Murdock, J.N., Wetzel, D.L., 2009. FT-IR Microspectroscopy Enhances Biological and  
 624 Ecological Analysis of Algae. *Appl. Spectrosc. Rev.* 44, 335–361.  
 625 <https://doi.org/10.1080/05704920902907440>

626 Napper, I.E., Davies, B.F.R., Clifford, H., Elvin, S., Koldewey, H.J., Mayewski, P.A., Miner,  
 627 K.R., Potocki, M., Elmore, A.C., Gajurel, A.P., Thompson, R.C., 2020. Reaching New  
 628 Heights in Plastic Pollution—Preliminary Findings of Microplastics on Mount Everest.  
 629 *One Earth* 3, 621–630. <https://doi.org/https://doi.org/10.1016/j.oneear.2020.10.020>

630 Pedrotti, M.L., Lombard, F., Baudena, A., Galgani, F., Elineau, A., Petit, S., Henry, M.,  
 631 Troublé, R., Reverdin, G., Ser-Giacomi, E., Kedzierski, M., Boss, E., Gorsky, G., 2022.  
 632 An integrative assessment of the plastic debris load in the Mediterranean Sea. *Sci. Total*  
 633 *Environ.* 838, 155958. <https://doi.org/https://doi.org/10.1016/j.scitotenv.2022.155958>

634 Prata, J.C., da Costa, J.P., Duarte, A.C., Rocha-Santos, T., 2019. Methods for sampling and  
 635 detection of microplastics in water and sediment: A critical review. *TrAC - Trends Anal.*

636 Chem. 110, 150–159. <https://doi.org/10.1016/j.trac.2018.10.029>

637 Primpke, S., Fischer, M., Lorenz, C., Gerdt, G., Scholz-Böttcher, B.M., 2020. Comparison of  
 638 pyrolysis gas chromatography/mass spectrometry and hyperspectral FTIR imaging  
 639 spectroscopy for the analysis of microplastics. Anal. Bioanal. Chem.  
 640 <https://doi.org/10.1007/s00216-020-02979-w>

641 Primpke, S., Wirth, M., Lorenz, C., Gerdt, G., 2018. Reference database design for the  
 642 automated analysis of microplastic samples based on Fourier transform infrared (FTIR)  
 643 spectroscopy. Anal. Bioanal. Chem. 410, 5131–5141. [https://doi.org/10.1007/s00216-](https://doi.org/10.1007/s00216-018-1156-x)  
 644 [018-1156-x](https://doi.org/10.1007/s00216-018-1156-x)

645 Quilès, F., Humbert, F., Delille, A., 2010. Analysis of changes in attenuated total reflection  
 646 FTIR fingerprints of *Pseudomonas fluorescens* from planktonic state to nascent biofilm  
 647 state. Spectrochim. Acta Part A Mol. Biomol. Spectrosc. 75, 610–616.  
 648 <https://doi.org/https://doi.org/10.1016/j.saa.2009.11.026>

649 Ramamoorthy, R., Vanitha, S., Krishnadev, P., Paramanathan, M., 2021. Synthesis and  
 650 characterization of phyto mediated talc-based nanocomposite by wet chemical reduction  
 651 method. Mater. Today Proc. <https://doi.org/https://doi.org/10.1016/j.matpr.2021.03.582>

652 Ripley, B.D., 1996. Pattern recognition and neural networks. Cambridge University Press,  
 653 Cambridge ; New York.

654 Scherer, C., Weber, A., Stock, F., Vurusic, S., Egerci, H., Kochleus, C., Arendt, N., Foeldi,  
 655 C., Dierkes, G., Wagner, M., Brennholt, N., Reifferscheid, G., 2020. Comparative  
 656 assessment of microplastics in water and sediment of a large European river. Sci. Total  
 657 Environ. 738, 139866. <https://doi.org/https://doi.org/10.1016/j.scitotenv.2020.139866>

658 Schmitt, J., Nivens, D., White, D.C., Flemming, H.-C., 1995. Changes of biofilm properties in

659 response to sorbed substances - an FTIR-ATR study. *Water Sci. Technol.* 32, 149–155.  
660 [https://doi.org/https://doi.org/10.1016/0273-1223\(96\)00019-4](https://doi.org/https://doi.org/10.1016/0273-1223(96)00019-4)

661 Schröder, E., Müller, G., Arndt, K.-F., 1989. *Polymer Characterization*. De Gruyter.

662 Schroeder, P., 2002. Infrared spectroscopy in clay science. *Teach. Clay Sci.* 11.

663 Schwarz, A., Ligthart, T., Boukris, E., Van Harmelen, T., 2019. Sources, transport, and  
664 accumulation of different types of plastic litter in aquatic environments: A review study  
665 ☆, *Marine Pollution Bulletin*. <https://doi.org/10.1016/j.marpolbul.2019.04.029>

666 Socrates, G., 2004. *Infrared and Raman Characteristic Group Frequencies: Tables and Charts*,  
667 3rd ed. John Wiley and Sons.

668 Stehfest, K., Toepel, J., Wilhelm, C., 2005. The application of micro-FTIR spectroscopy to  
669 analyze nutrient stress-related changes in biomass composition of phytoplankton algae.  
670 *Plant Physiol. Biochem.* 43, 717–726.  
671 <https://doi.org/https://doi.org/10.1016/j.plaphy.2005.07.001>

672 Sudhakar, K., Premalatha, M., 2015. Characterization of Micro Algal Biomass Through  
673 FTIR/TGA /CHN Analysis: Application to *Scenedesmus* sp. *Energy Sources, Part A*  
674 *Recover. Util. Environ. Eff.* 37, 2330–2337.  
675 <https://doi.org/10.1080/15567036.2013.825661>

676 Syranidou, E., Karkanorachaki, K., Amorotti, F., Franchini, M., Repouskou, E., Kaliva, M.,  
677 Vamvakaki, M., Kolvenbach, B., Fava, F., Corvini, P.F.-X., Kalogerakis, N., 2017.  
678 Biodegradation of weathered polystyrene films in seawater microcosms. *Sci. Rep.* 7,  
679 17991. <https://doi.org/10.1038/s41598-017-18366-y>

680 The R Core Team, 2019. *R: A Language and Environment for Statistical Computing*.

681 Venables, W.N., Ripley, B.D., Venables, W.N., 2002. *Modern applied statistics with S*, 4th

ed, Statistics and computing. Springer, New York.

Wakkaf, T., El Zrelli, R., Yacoubi, L., Kedzierski, M., Lin, Y.-J., Mansour, L., Bruzard, S., Rabaoui, L., 2022. Seasonal patterns of microplastics in surface sediments of a Mediterranean lagoon heavily impacted by human activities (Bizerte lagoon, Northern Tunisia). *Environ. Sci. Pollut. Res.* <https://doi.org/10.1007/s11356-022-21129-6>

Wang, J., Peng, J., Tan, Z., Gao, Y., Zhan, Z., Chen, Q., Cai, L., 2017. Microplastics in the surface sediments from the Beijiang River littoral zone: Composition, abundance, surface textures and interaction with heavy metals. *Chemosphere* 171, 248–258. <https://doi.org/10.1016/j.chemosphere.2016.12.074>

Wang, S., Wang, Y., Liang, Y., Cao, W., Sun, C., Ju, P., Zheng, L., 2020. The interactions between microplastic polyvinyl chloride and marine diatoms: Physiological, morphological, and growth effects. *Ecotoxicol. Environ. Saf.* 203, 111000. <https://doi.org/https://doi.org/10.1016/j.ecoenv.2020.111000>

Yagoubi, W., Abdelhafidi, A., Sebaa, M., Chabira, S.F., 2015. Identification of carbonyl species of weathered LDPE films by curve fitting and derivative analysis of IR spectra. *Polym. Test.* 44, 37–48. <https://doi.org/https://doi.org/10.1016/j.polymertesting.2015.03.008>

Yi, H., Zhao, Y., Liu, Y., Wang, W., Song, S., Liu, C., Li, H., Zhan, W., Liu, X., 2019. A novel method for surface wettability modification of talc through thermal treatment. *Appl. Clay Sci.* 176, 21–28. <https://doi.org/https://doi.org/10.1016/j.clay.2019.04.023>

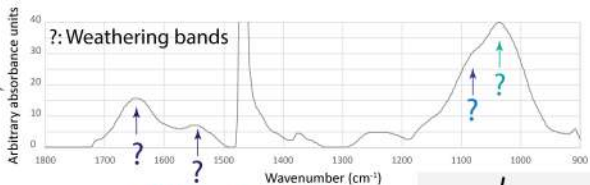
Zhang, K., Hamidian, A.H., Tubić, A., Zhang, Y., Fang, J.K.H., Wu, C., Lam, P.K.S., 2021. Understanding plastic degradation and microplastic formation in the environment: A review. *Environ. Pollut.* 274, 116554. <https://doi.org/https://doi.org/10.1016/j.envpol.2021.116554>

>4,000 microplastics

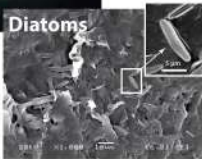
- PS  
- PE  
- PP



FTIR



SEM



Interpretations

- Algal proteins
- Si-O-Si bonds
- Algal polysaccharides

PE: Fouling indexes

$$FI = \frac{I_{1040-1020}}{I_{1480-1460}}$$

$$Fol = \frac{I_{1647-1627}}{I_{1480-1460}}$$